surfaces

MDPI

Article

Cyclic Voltammetry Characterization of Au, Pd, and AuPd Nanoparticles Supported on Different Carbon Nanofibers

Anna Testolin [1], Stefano Cattaneo [1], Wu Wang [2], Di Wang [2,3], Valentina Pifferi [1,*], Laura Prati [1], Luigi Falciola [1] and Alberto Villa [1,*]

1 Dipartimento di Chimica, Università degli Studi di Milano, Via Golgi 19, 20133 Milano, Italy; Anna.Testolin@unimi.it (A.T.); Stefano.Cattaneo2@unimi.it (S.C.); Laura.Prati@unimi.it (L.P.); luigi.falciola@unimi.it (L.F.)

2 Institute of Nanotechnology, Karlsruhe Institute of Technology, Hermann-von-Helmholtz-Platz 1, D-76344 Eggenstein-Leopoldshafen, Germany; wu.wang@partner.kit.edu (W.W.); di.wang@kit.edu (D.W.)

3 Karlsruhe Nano Micro Facility, Karlsruhe Institute of Technology, Hermann-von-Helmholtz-Platz 1, D-76344 Eggenstein-Leopoldshafen, Germany

* Correspondance: Valentina.Pifferi@unimi.it (V.P.); alberto.villa@unimi.it (A.V.); Tel.: +39-025-031-4222 (V.P.); +39-025-031-4361 (A.V.)

Received: 18 January 2019; Accepted: 13 March 2019; Published: 19 March 2019

Abstract: Three types of carbon nanofibers (pyrolytically stripped carbon nanofibers (PS), low-temperature heat treated carbon nanofibers (LHT), and high-temperature heat treated carbon nanofibers (HHT)) with different graphitization degrees and surface chemistry have been used as support for Au, Pd, or bimetallic AuPd alloy nanoparticles (NPs). The carbon supports have been characterized using Raman, X-ray photoelectron spectroscopy (XPS), and cyclic voltammetry (CV). Moreover, the morphology of the metal nanoparticles was investigated using transmission electron microscopy (TEM) and CV. The different properties of the carbon-based supports (particularly the graphitization degree) yield different electrochemical behaviors, in terms of potential window widths and electrocatalytic effects. Comparing the electrochemical behavior of monometallic Au and Pd and bimetallic AuPd, it is possible to observe the interaction of the two metals when alloyed. Moreover, we demonstrate that carbon surface has a strong effect on the electrochemical stability of AuPd nanoparticles. By tuning the Au-Pd nanoparticles' morphology and modulating the surface chemistry of the carbon support, it is possible to obtain materials characterized by novel electrochemical properties. This aspect makes them good candidates to be conveniently applied in different fields.

Keywords: gold; palladium; bimetallic alloy; carbon nanofibers (CNFs); cyclic voltammetry (CV)

1. Introduction

Over the last decades, many studies have focused on metal nanoparticles, thanks to their excellent catalytic, electrocatalytic, optical, and magnetic properties, that often differ from the ones of their correspondent bulk metals [1–3]. There has also been interest in bimetallic nanosystems, because of the possibility to create new materials characterized by specific and innovative properties due to synergistic effects among precursors [4–7]. These effects reflect a general enhancement of the performances of the final products with respect to their monometallic components. The possibility to have different kinds of bimetallic samples (in terms of composition, structure, metal loading, morphology, etc.) has led to widespread applications in a lot of fields such as engineering, electronics, catalysis, electrocatalysis, and sensors [8–10]. Particularly in heterogeneous catalysis and electrocatalysis, metal nanoparticles are often supported on specific substrates [11–17], which in turn possess different characteristics and

properties related to the amount of catalyst loaded on the solid material, or to the different nature and functionalization of the substrate itself. However, in many cases, the effect of the support on the properties of the metal nanoparticles and the possible synergistic effects between bimetallic composites and supports are yet to be investigated in depth.

In the present work, we propose an integrated study of three types of carbon nanofibers (PS, LHT, and HHT) modified with Au and/or Pd nanoparticles (AuNPs, PdNPs, and alloyed AuPdNPs). AuPd systems are widely used in electrocatalysis due to their peculiar behavior compared to the corresponding monometallic Au and Pd [18–23]. Besides surface characterization techniques, such as Raman, TEM, and XPS, commonly involved in the study of these kind of materials [24,25], cyclic voltammetry is here used as a supplementary and complementary characterization method [26–29]. The different properties of the supports, particularly in terms of graphitization degree, are reflected in different electrochemical behaviors, in terms of potential window widths, electrocatalytic effects, and preferential sites for anchoring the nanoparticles. Moreover, the results highlight how the bimetallic samples behave differently with respect to the relative Au and Pd monometallic systems, underlying the presence of an intimate contact between the two metals, which provides new materials, completely different from the original ones. This aspect makes them good candidates to be conveniently applied in many different applications.

2. Materials and Methods

2.1. Metal Nanoparticles/CNFs Preparation

Commercial carbon nanofibers (CNFs), PR24-PS (hereafter shortened as PS) from Applied Sciences, inc. (average diameter of 100 ± 30 nm and a specific surface area of 45 m^2/g); CNFs PR24-LHT (LHT) from Applied Sciences, inc. (average diameter of 100 ± 30 nm and a specific surface area of 43 m^2/g); and CNFs PR24-HHT (HHT) from Applied Sciences, inc. (average diameter of 100 ± 30 nm and a specific surface area of 41 m^2/g) were used as pristine carbon materials. $NaAuCl_4$*$2H_2O$ (99%, Aldrich, St. Louis, MO, USA) and Na_2PdCl_4 (98 % Aldrich) were used as metal precursors, while $NaBH_4$ (> 98%, Ventron) and polyvinyl alcohol (PVA, MW = 9000–10,000, 80 % hydrolyzed, Aldrich) were used as reducing and protective agents, respectively.

AuNPs: 0.051 mol of solid $NaAuCl_4$ *$2H_2O$ and PVA solution (1% w/w, metal/PVA 1:1 w/w) were added to 100 mL of Milli-Q H_2O. The solution was stirred for few minutes, after which $NaBH_4$ (metal/$NaBH_4$ = 1/4 mol/mol) solution was added under vigorous magnetic stirring. Within a few minutes of sol generation, the sol was immobilized by adding the support (ca. 1 g) under vigorous stirring. The slurry was filtered, and the catalyst washed thoroughly with distilled water and dried at 80 °C for 4 h. The total nominal metal loading was 1 wt %.

PdNPs: 0.094 mol of Na_2PdCl_4 and PVA solution (1% w/w, metal/PVA 1:1 w/w) were added to 100 mL of Milli-Q H_2O. The solution was stirred for few minutes, after which $NaBH_4$ (metal/$NaBH_4$ = 1/8 mol/mol) solution was added under vigorous magnetic stirring. Within a few minutes of sol generation, the sol was immobilized by adding the support (ca. 1 g) under vigorous stirring. The slurry was filtered, and the catalyst washed thoroughly with distilled water and dried at 80 °C for 4 h. The total nominal metal loading was 1 wt %.

AuPdNPs: 0.037 mol of solid $NaAuCl_4$ *$2H_2O$, 0.025 mol of Na_2PdCl_4 and PVA solution (1% w/w, metal/PVA 1:1 w/w) were added to 100 mL of Milli-Q H_2O. The yellow solution was stirred for few minutes, after which $NaBH_4$ (metal/$NaBH_4$ = 1/8 mol/mol) solution was added under vigorous magnetic stirring. Within a few minutes of sol generation, the sol was immobilized by adding the support (ca. 1 g) under vigorous stirring. The slurry was filtered, and the catalyst washed thoroughly with distilled water and dried at 80 °C for 4 h. The total nominal metal loading was 1 wt %.

2.2. Electrochemical Characterization

Cyclic voltammetric experiments were performed using an AutoLab PGStat128 (Metrohm AutoLab, Utrecht, The Netherlands) equipped with the NOVA 2.1 Software (Metrohm AutoLab, Utrecht, The Netherlands). The experimental setting was composed of a conventional three electrodes cell in which a saturated calomel electrode and a platinum wire were used as reference (RE) and counter (CE) electrodes, respectively. A glassy carbon (GC) modified with carbon nanofibers (CNFs) or with mono or bimetallic Au and Pd NPs supported on carbon nanofibers was used as working electrode (WE). Before the modification, GC was polished with diamond powder (1 µm, Sigma Aldrich, Milan, Italy) on a Struers DP-Nap cloth and washed with milli-Q water. 5 mg of the different CNF-NPs powders were suspended in 1 mL EtOH (96 %, Sigma Aldrich) and 4.5 µL Nafion (5% solution in low aliphatic alcohols, Aldrich, Milan, Italy). Then, 20 µL of the suspension was deposited on GC using an automatic micropipette (Kartell, Noviglio, Milan, Italy) and allowed to dry for approximately 30 min. Cyclic voltammetries were recorded in aqueous solution with 0.1 M H_2SO_4 as supporting electrolyte. The potential was scanned from −1 V (SCE) to +2 V (SCE), at a scan rate of 100 mV s^{-1} and a step potential of 5 mV.

2.3. Morphological Characterization

Raman spectroscopy was performed with a Renishaw inVia Raman microscope for analysing the graphitisation degree of the carbon nanofibers. Bare supports and fresh and used catalysts were analysed. Typically, a sample of approximately 0.01 g was placed on a metal slide inside the spectrometer. The powder was analysed under an IR class laser (514 nm) with a laser intensity of 50 %. The sample was scanned at an attenuation time of 22 seconds, and 10 scans were carried out to give a spectrum.

X-ray photoelectron spectroscopy (XPS) was performed on a Thermo Scientific K-alpha+ spectrometer (Thermo Fisher Scientific, Waltham, MA, USA). Samples were analysed using a monochromatic Al x-ray source operating at 72 W (6 mA × 12 kV), with the signal averaged over an oval-shaped area of approximately 600 × 400 microns. Data were recorded at pass energies of 150 eV for survey scans and 40 eV for high resolution scan with a 1eV and 0.1 eV step size, respectively. Charge neutralization of the sample was achieved using a combination of both low energy electrons and argon ions (less than 1 eV), which gave a C(1s) binding energy of 284.8 eV.

All data were analysed using CasaXPS (v2.3.17 PR1.1) using Scofield sensitivity factors and an energy exponent of −0.6.

The Au, Pd specimens were characterized by transmission electron microscopy (TEM, FEI Titan 80−300, Thermo Fisher Scientific, Waltham, MA, USA). The samples were directly dispersed on copper grids covered with holey carbon film. Morphology of the catalysts was characterized by high angle annular dark-field (HAADF) scanning transmission electron microscopy (STEM), and its composition information was acquired by EDAX S-UTW EDX detector in an FEI Titan 80−300 microscope operating (Thermo Fisher Scientific, Waltham, MA, USA) at 300 kV. Analysis of STEM-EDX spectrum imaging was carried out by using TEM image and analysis (TIA 4.7 SP3 version) software. Particle size of the specimens was measured on HAADF-STEM images by using the ImageJ software (National Institutes of Health, Bethesda, MD, USA) fitting the particles with ellipsoid shapes.

3. Results and Discussion

3.1. Morphological Characterization

Commercial carbon nanofibers (CNFs) thermally processed at different severity degrees [30,31], were selected as supports. Raman spectroscopy has been used to investigate the graphitization degree of CNFs treated at different temperatures. In particular, the ratio of the integral intensities of D and G bands (I_D/I_G), which is an index of the defectiveness of the graphite layers [32], was measured (Table 1). G band is related to structurally-ordered graphite domains, whereas D band can be associated

with the turbostratic and/or disordered carbonaceous structures [32]. As expected, increasing the temperature of the heat treatment results in a higher graphitization degree (I_D/I_G = 0.75, 0.60, 0.11 for PS, LHT, HHT, respectively) (Table 1). X-ray photoelectron spectroscopy (XPS) has been used to confirm the different graphitization degrees. C1s XPS spectra show two main components: the first one at 284 eV, which can be attributed to sp^2-hybridised carbon species, and the second component at 285 eV ascribable to the presence of sp^3-hybridised carbon species [33] (Figure 1 and Tables 1 and 2). Sp^2/sp^3 increased with increasing annealing temperature (4.1, 7.0 and 16.8 for PS, LHT, HHT, respectively) (Table 1). Accordingly, a higher amount of oxygen has been observed decreasing the graphitization degree (C:O ratio of 88.3:11.7, 92.2:7.8, 97.3:2.7 for PS, LHT, HHT, respectively) (Table 2). Table 2 summarizes the oxygen species observed on the surface, their concentration, and the overall elemental composition. Fitting the O1s peak, five contributions were observed (Figure 2). Binding Energy (BE) of 530.2–530.5 eV corresponds to highly conjugated forms of carbonyl oxygen such as quinone [34]. The second contribution (531.6-531.9 eV) can be assigned to a carbon–oxygen double bond, whereas the one at 533.0-533.5 eV corresponds to an ether-like single bond C-O-C and to carbon oxygen single-bonds in hydroxyl groups C-O-H [35]. Oxygen species at 534.6–535.0 eV refers to the presence of carboxylic groups COOH [35]. The last signal at 536.7–537.1 eV can be assigned to adsorbed water [36]. C=O, C-O-H and C-O-C were the most abundant species present in all the CNFs (Table 2 and Figure 2).

Table 1. Atomic content of sp^2 and sp^3 carbon and ratio sp^2/sp^3 from X-ray photoelectron spectroscopy (XPS) and I_D/I_G ratio from Raman for the bare supports.

Catalyst	C sp^2 (%)	C sp^3 (%)	sp^2/sp^3	I_D/I_G
PS	75.8	18.6	4.1	0.75
LHT	83.8	12.0	7.0	0.60
HHT	90.8	3.4	16.8	0.11

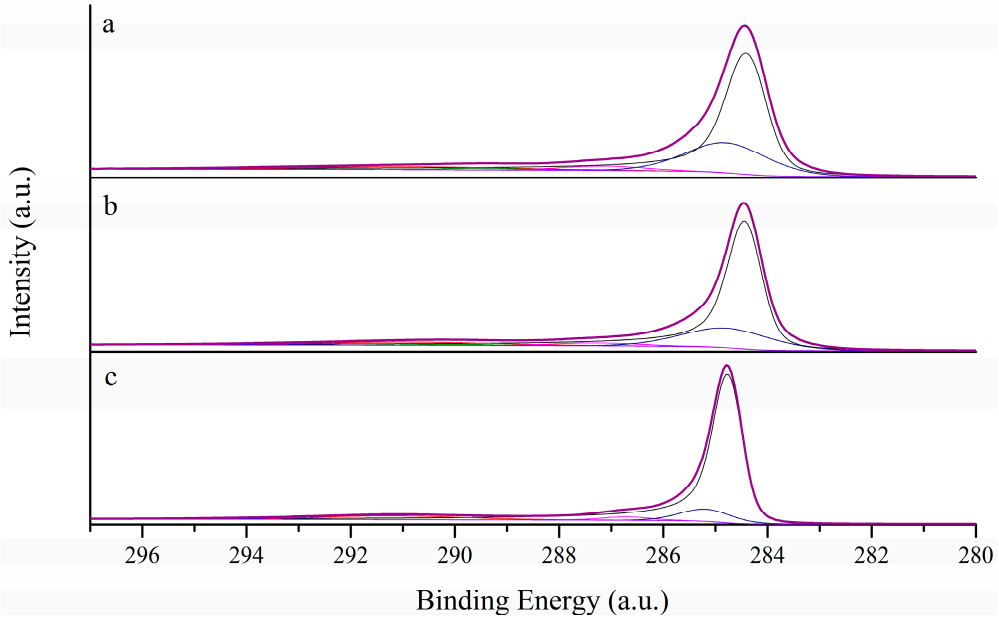

Figure 1. C1s XPS spectra of (**a**) pyrolytically stripped carbon nanofibers (PS), (**b**) low-temperature heat treated carbon nanofibers (LHT), and (**c**) high-temperature heat treated carbon nanofibers (HHT).

Table 2. XPS analysis of the carbon nanofibers (CNFs).

Sample		O1S					C1s				Atomic Ratio % C:O
		C = O	C-O-H	C-O-C	COOH	H_2O	sp^2	sp^3	C = O	C = C	
PS	BE	530.2	531.8	533.0	534.6	536.7	284.4	284.9	287.2	290.0	88.3:11.7
	Atom %	(10.2)	(40.7)	(33.1)	(9.8)	(6.0)	(75.8)	(18.6)	(3.7)	(1.8)	
LHT	BE	530.5	531.6	533.1	535.0	537.1	284.5	284.9	287.4	290.1	92.2:7.8
	Atom %	(11.6)	(34.2)	(40.3)	(8.8)	(5.1)	(83.8)	(12.0)	(2.6)	(1.6)	
HHT	BE	530.2	531.9	533.5	535.0	537.0	284.7	285.2	287.9	290.6	97.3:2.7
	Atom %	(13.9)	(46.2)	(24.0)	(10.1)	(5.8)	(90.8)	(5.4)	(1.6)	(2.2)	

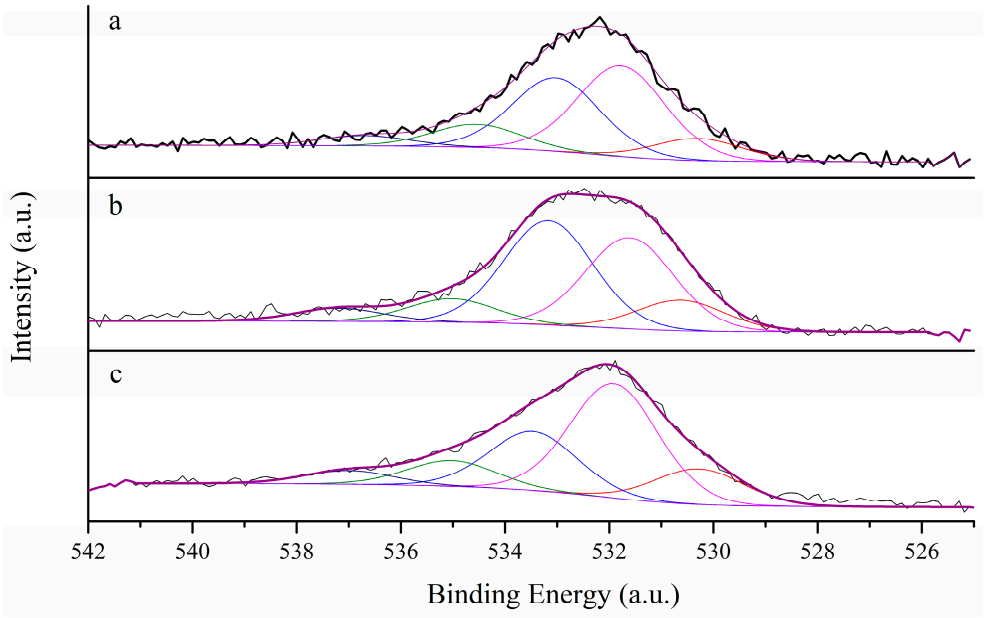

Figure 2. O1s XPS spectra of (**a**) PS, (**b**) LHT, and (**c**) HHT.

Monometallic Au and Pd, together with their corresponding bimetallic system (AuPd), were prepared by sol immobilization method using polyvinyl alcohol (PVA) as protective agent and $NaBH_4$ as reducing agent and immobilized on the three different CNFs. The monometallic and bimetallic systems consist of nanoparticles with an average size of 3–4 nm [37,38]. To investigate the morphology of the bimetallic systems, STEM-EDX spectrum imaging was performed on single nanoparticles to map the interior metal compositions. Element maps of one AuPd particle are reported in Figure 3, as example. Both Pd and Au signals were found in nanoparticles with a similar distribution, indicating the formation of AuPd alloyed nanoparticles. Quantification of the integrated EDX spectra of this nanoparticle indicates that the atomic ratio of Au and Pd is 64/36 close to the nominal 60/40 (Figure 3).

3.2. Electrochemical Characterization

As demonstrated by Raman spectra and XPS analysis (see Tables 1 and 2, Figures 1 and 2 in Section 3.1), the three types of carbon nanofibers differ in the ratio between the sp^2 and sp^3 conformation of carbon atoms, i.e., in the "graphitization" degree, an index of the order degree in carbon-based materials [31,39,40]. These differences are reflected in different voltammetric behaviours, especially in terms of potential window widths (the useful voltage range, between the upper and lower limits where oxidation and reduction of the solvent/supporting electrolyte occur) and electro-catalytic effects (Figure 4).

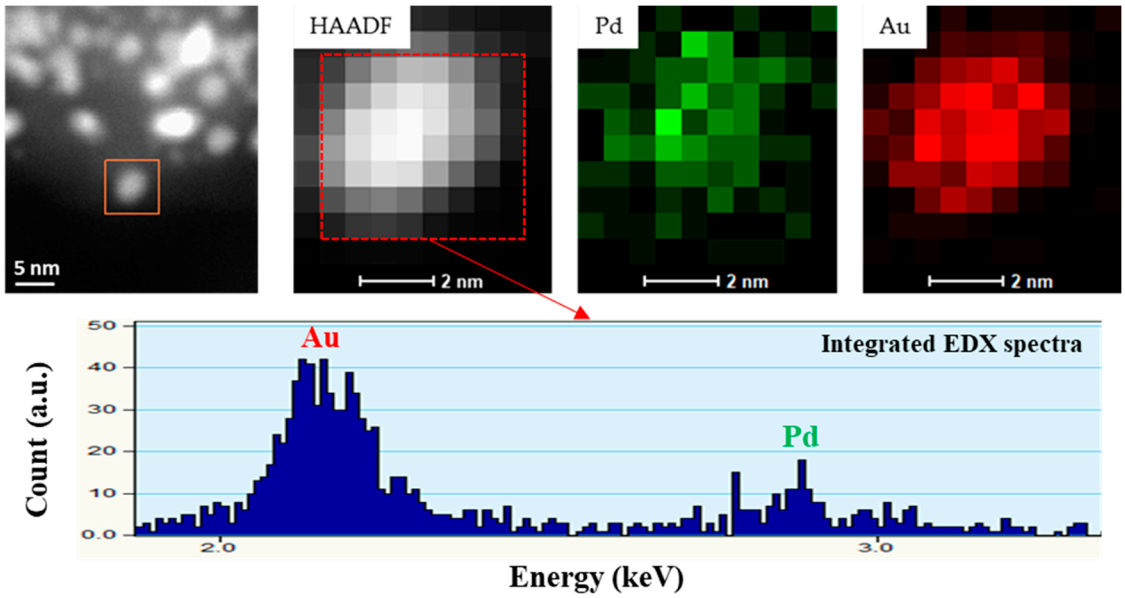

Figure 3. The element maps obtained from Scanning Electron Microscopy- Energy Dispersive X-ray Analysis (STEM)-EDX spectrum imaging in the area marked box of AuPd nanoparticles and the integrated EDX spectra of this nanoparticle.

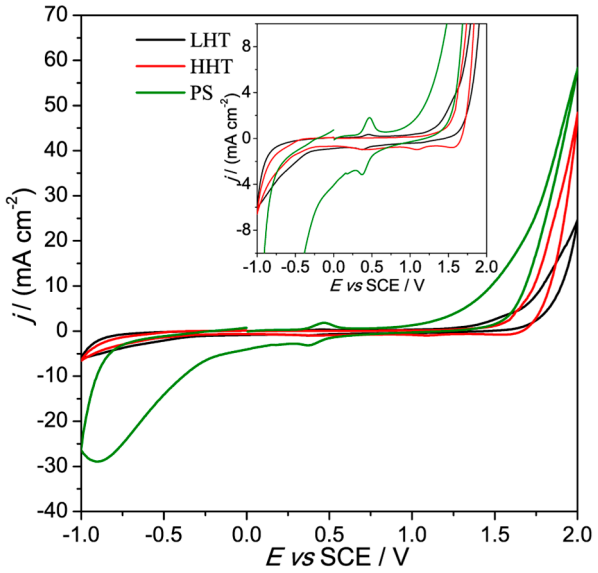

Figure 4. Cyclic voltammetry (CV) patterns of PS, LHT, and HHT nanofibers recorded in 0.1 M H_2SO_4 at 100 mV s^{-1}. Zoom of the current density values in the inset.

The potential window width is in the order PS < LHT < HHT (Figure 4), both in the cathodic and anodic side, pointing out the higher electrochemical stability and inertness of HHT (> LHT > PS) towards oxygen evolution reaction (OER, in the anodic side) and hydrogen evolution reaction (HER, in the cathodic side).

Moreover, PS nanofibers present oxidation and reduction peaks around +0.4 V (SCE), which are less marked for LHT and basically absent in the case of HHT. Considering the surface morphology of the investigated materials (Section 3.1), these peaks have been attributed to the presence of oxygen functionalizations on the nanofibers [41,42], which are in higher concentrations in the case of PS, lower for LHT, and almost absent in HHT (Table 2). It is known, in fact, that the lower the graphitization degree, the higher the presence of surface impurities and defects [43]. The presence of these functionalities can be responsible also for the different potential windows of the materials.

In order to investigate if the various properties of the nanofibers reflect also in a different behavior when they are used as support for the nanoparticles samples, we studied CNFs modified with monometallic Au or Pd NPs and with bimetallic AuPd alloyed NPs.

Figure 5a reports the voltammograms of the Au-modified nanofibers. As previously observed in Figure 4, the smallest potential window is related to PS system, followed by LHT and then HHT. In this case, however, additional oxidation and reduction peaks related to the presence of gold nanoparticles on the carbonaceous fibers are present (inset of Figure 5A). In particular, apart from the same peaks of the bare nanofibers at +0.4 V (SCE), a well-defined signal (for LHT and HHT) at around +1.3 V (SCE) is evident, whose peak-shape confirms the nanosized structure of the Au particles [44]. In the case of PS, the signal is partially covered by the reaction of the background, resulting in a shoulder plateau. Considering the oxidation peak potential position, a small catalytic effect for HHT (peak at +1.25 V vs SCE, with respect to the value of +1.31 for LHT-supported sample) is observed, probably related to a higher interaction between HHT nanofiber and AuNPs, due to the high graphitization degree of the material which reflects in a favored electron transfer.

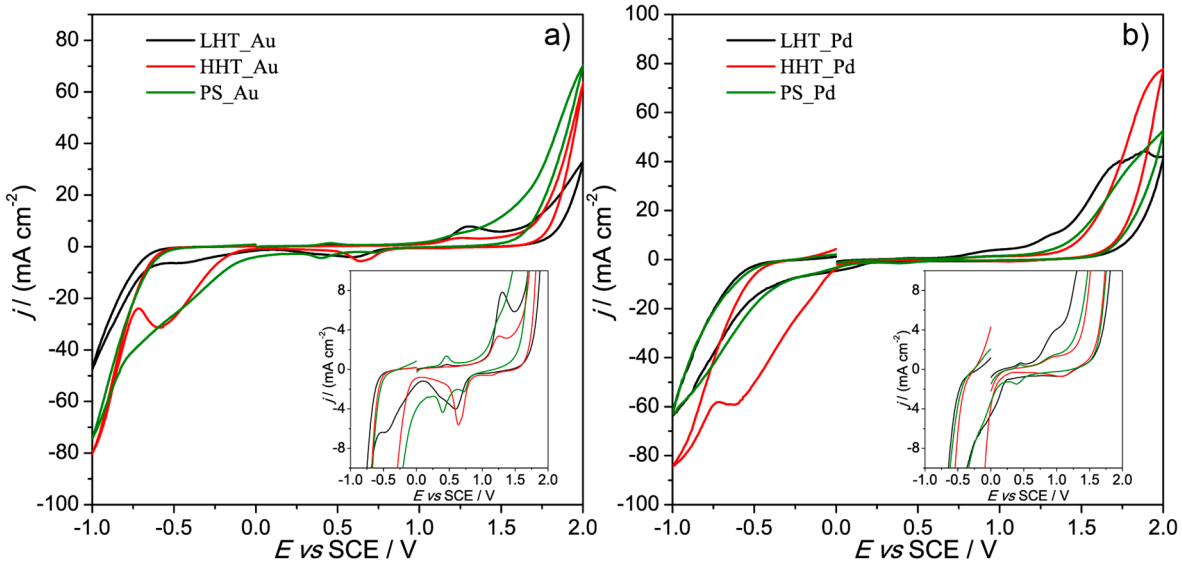

Figure 5. Cyclic voltammetry (CV) of PS, LHT, and HHT modified with AuNPs (**a**) or PdNPs (**b**) recorded in H_2SO_4 0.1 M at 100 mV s^{-1}. In the inset, zoom on the density current values.

The interesting behavior of the supported materials can be outlined considering the main oxide-reduction peaks in the 0.5–0.8 V (SCE) region, to be compared with the peak position (at about +0.8 V (SCE)) of analogous AuNPs system in the absence of the carbon nanofibers support [40]. In the present case, all the three different supported samples show the gold oxide reduction peaks at lower potentials (and in the order PS < LHT < HHT). This behavior can be ascribed to a different electrochemical stabilizing effect exhibited by the different carbonaceous fibers on the nanomaterials that can be further and conveniently exploited in sensing and catalytic applications.

In the case of PdNPs (Figure 5b), the presence of a small oxidation peak around +1 V (SCE) is evident, which is in line with the values of analogous colloidal PdNPs. In the case of LHT_Pd, more intense signals at about 1.73 and 1.89 V (SCE) are present, probably due to the concomitant Pd over-oxidation together with O_2 evolution. In both HHT systems (HHT_Au and HHT_Pd), an evident reduction peak at about −0.6 V (SCE) is present, whose nature is yet to be clarified (Figure S1).

The CV patterns of the bimetallic alloyed AuPd nanoparticles supported on the carbonaceous materials (Figure 6) are more interesting. Also in this case, the broad oxidation peak related to the reaction of the background is present in the PS fibers case, which covers the ones related to the metallic nanoparticles. In the case of LHT, it can be noticed the presence of two oxidation peaks at about +1.25 and +1.74 V (SCE) related to the Pd and Au oxide formation, respectively, both shifted at higher anodic

potentials with respect to their monometallic components [45]. This behavior can be attributed to a stabilizing effect that the two metals exhibit when they are alloyed, as already evidenced in the literature [7]. The single reduction signal at about −0.29 V (SCE) is probably related to the reduction of the alloyed AuPd oxide, which occurs at a more cathodically shifted potential with respect to its monometallic references, resulting in a great stabilization of the oxide, probably due to the synergistic effects of the two metals in the alloy, and also due to a contribution by the carbonaceous support. This unexpected potential shift of the main oxide-reduction peak (usually, on bare Pd, in this region it is more likely to have proton absorption), has been observed in other homogeneous noble metals alloys [46] and in other bimetallic Pd-based catalysts supported on carbon nanofibers [47].

For HHT, a small oxidation peak around +1.2 V (SCE) is present (see the inset of Figure 6), which could be related to the formation of the palladium oxide, but no signal related to the oxidation of AuNPs is evident. It seems that the AuNPs oxidation process occurs at higher potential with respect to +2 V (SCE), where the signal of the OER takes place. Also, the reduction peak in this case is not evident (probably extremely cathodically shifted and under the signal of the HER background), once more evidencing the greater stabilizing effect of HHT on the alloyed NPs.

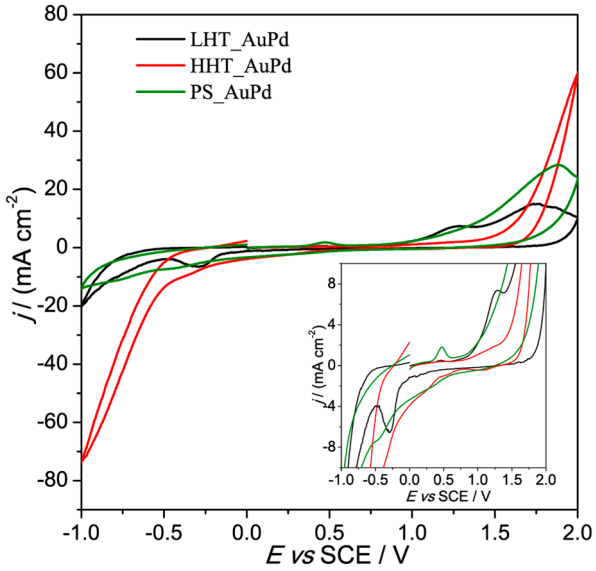

Figure 6. Cyclic voltammetric (CV) features of PS, LHT, and HHT modified with AuPdNPs recorded in H_2SO_4 0.1 M at 100 mV s^{-1}. Zoom of the density current values in the insets.

4. Conclusions

Three types of carbon nanofibers (PS, LHT, and HHT) characterized by a different degree of graphitization (HHT > LHT > PS) have been studied by CV. The different properties of the carbon-based supports yield different electrochemical behaviors, in terms of potential window widths and electrocatalytic effects. Au, Pd, and bimetallic AuPd alloy nanoparticles have been prepared by sol immobilization using PVA as a stabilizer and $NaBH_4$ as a reducer, and deposited on the three carbon nanofibers. The subsequent support of the metal NPs yields the different behavior of the latter in comparison to the non-supported systems. A cathodic and anodic shift in the oxidation and reduction peaks, related to the formation and disruption of the oxide, is evident, particularly in the case of the use of the more graphitized HHT support. This effect can be attributed to a different interaction between the metal systems and the carbon supports, which provides devices characterized by the presence of the metal catalyst, but with unexpected large potential windows, to be conveniently used in electrocatalysis and sensors applications.

Supplementary Materials: The following are available online at http://www.mdpi.com/2571-9637/2/1/16/s1, Figure S1: Cyclic Voltammetric (CV) features of HHT nanofibers modified with Au, Pd and AuPdNPs recorded in H_2SO_4 0.1 M at 100 mV s^{-1}.

Author Contributions: V.P. and A.V. designed the experiments; A.T. performed the CV experiments and wrote the article; A.V. carried out the XPS experiments and helped in the interpretation; W.W. and D.W. carried out the TEM experiments and helped in the interpretation; V.P. and L.F. helped in the interpretation of the CV results; S.C. prepared the materials; and L.P. and L.F. were involved in the writing and editing of the manuscript.

Acknowledgments: We acknowledge Karlsruhe Nano Micro Facility for using the TEM.

Conflicts of Interest: The authors declare no conflict of interest.

References

1. Campbell, F.W.; Compton, R.G. The use of nanoparticles in electroanalysis: An updated review. *Anal. Bioanal. Chem.* **2010**, *396*, 241–259. [CrossRef]
2. Sardar, R.; Funston, A.M.; Mulvaney, P.; Murray, R.W. Gold Nanoparticles: Past, Present, and Future. *Langmuir* **2009**, *25*, 13840–13851. [CrossRef] [PubMed]
3. Silvestri, A.; Mondini, S.; Marelli, M.; Pifferi, V.; Falciola, L.; Ponti, A.; Ferretti, A.M.; Polito, L. Synthesis of Water Dispersible and Catalytically Active Gold-Decorated Cobalt Ferrite Nanoparticles. *Langmuir* **2016**, *32*, 7117–7126. [CrossRef]
4. Rodriguez, J.A.; Goodman, D.W. The nature of the metal-metal bond in bimetallic surfaces. *Science* **1992**, *257*, 897–903. [CrossRef] [PubMed]
5. Toshima, N.; Yonezawa, T. Bimetallic nanoparticles—Novel materials for chemical and physical applications. *New J. Chem.* **1998**, *22*, 1179–1201. [CrossRef]
6. Sankar, M.; Dimitratos, N.; Miedziak, P.J.; Wells, P.P.; Kiely, C.J.; Hutchings, G.J. Designing bimetallic catalysts for a green and sustainable future. *Chem. Soc. Rev.* **2012**, *41*, 8099–8139. [CrossRef] [PubMed]
7. Villa, A.; Wang, D.; Su, D.S.; Prati, L. New challenges in gold catalysis: Bimetallic systems. *Catal. Sci. Technol.* **2015**, *5*, 55–68. [CrossRef]
8. Schrinner, M.; Proch, S.; Mei, Y.; Kempe, R.; Miyajima, N.; Ballauff, M. Stable Bimetallic Gold–Platinum Nanoparticles Immobilized on Spherical Polyelectrolyte Brushes: Synthesis, Characterization, and Application for the Oxidation of Alcohols. *Adv. Mater.* **2008**, *20*, 1928–1933. [CrossRef]
9. Kim, C.; Dionigi, F.; Beermann, V.; Wang, X.; Möller, T.; Strasser, P. Alloy Nanocatalysts for the Electrochemical Oxygen Reduction (ORR) and the Direct Electrochemical Carbon Dioxide Reduction Reaction (CO_2 RR). *Adv. Mater.* **2018**, 1805617. [CrossRef]
10. Hu, Y.; Zhang, H.; Wu, P.; Zhang, H.; Zhou, B.; Cai, C. Bimetallic Pt-Au nanocatalysts electrochemically deposited on graphene and their electrocatalytic characteristics towards oxygen reduction and methanol oxidation. *Phys. Chem. Chem. Phys.* **2011**, *13*, 4083–4094. [CrossRef]
11. Liu, X.Y.; Wang, A.; Zhang, T.; Mou, C.Y. Catalysis by gold: New insights into the support effect. *Nano Today* **2013**, *8*, 403–416. [CrossRef]
12. Bracey, C.L.; Ellis, P.R.; Hutchings, G.J. Application of copper-gold alloys in catalysis: Current status and future perspectives. *Chem. Soc. Rev.* **2009**, *38*, 2231–2243. [CrossRef]
13. Gliech, M.; Klingenhof, M.; Görlin, M.; Strasser, P. Supported metal oxide nanoparticle electrocatalysts: How immobilization affects catalytic performance. *Appl. Catal. A Gen.* **2018**, *568*, 11–15. [CrossRef]
14. Zhang, J.W.; Sun, K.K.; Li, D.D.; Deng, T.; Lu, G.P.; Cai, C. Pd-Ni bimetallic nanoparticles supported on active carbon as an efficient catalyst for hydrodeoxygenation of aldehydes. *Appl. Catal. A Gen.* **2019**, *569*, 190–195. [CrossRef]
15. Peneau, V.; He, Q.; Shaw, G.; Kondrat, S.A.; Davies, T.E.; Miedziak, P.; Forde, M.; Dimitratos, N.; Kiely, C.J.; Hutchings, G.J. Selective catalytic oxidation using supported gold-platinum and palladium-platinum nanoalloys prepared by sol-immobilisation. *Phys. Chem. Chem. Phys.* **2013**, *15*, 10636–10644. [CrossRef] [PubMed]
16. Rodriguez, R.C.; Moncada, A.B.; Acevedo, D.F.; Planes, G.A.; Miras, M.C.; Barbero, C.A. Electroanalysis using modified hierarchical nanoporous carbon materials. *Faraday Discuss.* **2013**, *164*, 147. [CrossRef] [PubMed]

17. Villa, A.; Schiavoni, M.; Prati, L. Material science for the support design: A powerful challenge for catalysis. *Catal. Sci. Technol.* **2012**, *2*. [CrossRef]
18. Romero Hernández, A.; Manríquez, M.E.; Ezeta Mejia, A.; Arce Estrada, E.M. Shape Effect of AuPd Core-Shell Nanostructures on the Electrocatalytical Activity for Oxygen Reduction Reaction in Acid Medium. *Electrocatalysis* **2018**, *9*, 752–761. [CrossRef]
19. Yang, J.; Deng, S.; Lei, J.; Ju, H.; Gunasekaran, S. Electrochemical synthesis of reduced graphene sheet-AuPd alloy nanoparticle composites for enzymatic biosensing. *Biosens. Bioelectron.* **2011**, *29*, 159–166. [CrossRef]
20. Jin, C.; Wan, C.; Dong, R. Electrocatalytic Activity Enhancement of Pd Nanoparticles Supported on Reduced Graphene Oxide by Surface Modification with Au. *J. Electrochem. Soc.* **2017**, *164*, H696–H700. [CrossRef]
21. Shang, L.; Zhao, F.; Zeng, B. Sensitive voltammetric determination of vanillin with an AuPd nanoparticles-graphene composite modified electrode. *Food Chem.* **2014**, *151*, 53–57. [CrossRef] [PubMed]
22. Mueller, J.E.; Krtil, P.; Kibler, L.A.; Jacob, T. Bimetallic alloys in action: Dynamic atomistic motifs for electrochemistry and catalysis. *Phys. Chem. Chem. Phys.* **2014**, *16*, 15029–15042. [CrossRef] [PubMed]
23. Pluntke, Y.; Kibler, L.A.; Kolb, D.M. Unique activity of Pd monomers: Hydrogen evolution at AuPd(111) surface alloys. *Phys. Chem. Chem. Phys.* **2008**, *10*, 3684–3688. [CrossRef] [PubMed]
24. Baer, D.R.; Amonette, J.E.; Engelhard, M.H.; Gaspar, D.J.; Karakoti, A.S.; Kuchibhatla, S.; Nachimuthu, P.; Nurmi, J.T.; Qiang, Y.; Sarathy, V.; et al. Characterization challenges for nanomaterials. In *Surface and Interface Analysis*; John Wiley & Sons, Ltd.: Hoboken, NJ, USA, 2008; Volume 40, pp. 529–537.
25. Villa, A.; Dimitratos, N.; Chan-Thaw, C.E.; Hammond, C.; Veith, G.M.; Wang, D.; Manzoli, M.; Prati, L.; Hutchings, G.J. Characterisation of gold catalysts. *Chem. Soc. Rev.* **2016**, *45*. [CrossRef] [PubMed]
26. Holt, L.R.; Plowman, B.J.; Young, N.P.; Tschulik, K.; Compton, R.G. The Electrochemical Characterization of Single Core-Shell Nanoparticles. *Angew. Chem. Int. Ed.* **2016**, *55*, 397–400. [CrossRef] [PubMed]
27. Plowman, B.J.; Sidhureddy, B.; Sokolov, S.V.; Young, N.P.; Chen, A.; Compton, R.G. Electrochemical Behavior of Gold–Silver Alloy Nanoparticles. *ChemElectroChem* **2016**, *3*, 1039–1043. [CrossRef]
28. Tschulik, K.; Ngamchuea, K.; Ziegler, C.; Beier, M.G.; Damm, C.; Eychmueller, A.; Compton, R.G. Core-Shell Nanoparticles: Characterizing Multifunctional Materials beyond Imaging—Distinguishing and Quantifying Perfect and Broken Shells. *Adv. Funct. Mater.* **2015**, *25*, 5149–5158. [CrossRef]
29. Ranđelović, M.; Momčilović, M.; Matović, B.; Babić, B.; Barek, J. Cyclic voltammetry as a tool for model testing of catalytic Pt- and Ag-doped carbon microspheres. *J. Electroanal. Chem.* **2015**, *757*, 176–182. [CrossRef]
30. Tessonnier, J.P.; Rosenthal, D.; Hansen, T.W.; Hess, C.; Schuster, M.E.; Blume, R.; Girgsdies, F.; Pfänder, N.; Timpe, O.; Su, D.S.; et al. Analysis of the structure and chemical properties of some commercial carbon nanostructures. *Carbon N. Y.* **2009**, *47*, 1779–1798. [CrossRef]
31. Campisi, S.; Sanchez Trujillo, F.; Motta, D.; Davies, T.; Dimitratos, N.; Villa, A. Controlling the Incorporation of Phosphorus Functionalities on Carbon Nanofibers: Effects on the Catalytic Performance of Fructose Dehydration. *C* **2018**, *4*, 9. [CrossRef]
32. Tuinstra, F.; Koenig, J.L. Raman Spectrum of Graphite. *J. Chem. Phys.* **1970**, *53*, 1126–1130. [CrossRef]
33. Xie, F.Y.; Xie, W.G.; Gong, L.; Zhang, W.H.; Chen, S.H.; Zhang, Q.Z.; Chen, J. Surface characterization on graphitization of nanodiamond powder annealed in nitrogen ambient. *Surf. Interface Anal.* **2010**, *42*, 1514–1518. [CrossRef]
34. Martínez, M.T.; Callejas, M.A.; Benito, A.M.; Cochet, M.; Seeger, T.; Ansón, A.; Schreiber, J.; Gordon, C.; Marhic, C.; Chauvet, O.; et al. Sensitivity of single wall carbon nanotubes to oxidative processing: Structural modification, intercalation and functionalisation. *Carbon N. Y.* **2003**, *41*, 2247–2256. [CrossRef]
35. Figueiredo, J.L.; Pereira, M.F.R.; Freitas, M.M.A.; Órfão, J.J.M. Modification of the surface chemistry of activated carbons. *Carbon N. Y.* **1999**, *37*, 1379–1389. [CrossRef]
36. Ketteler, G.; Ashby, P.; Mun, B.S.; Ratera, I.; Bluhm, H.; Kasemo, B.; Salmeron, M. In situ photoelectron spectroscopy study of water adsorption on model biomaterial surfaces. *J. Phys. Condens. Matter* **2008**, *20*, 184024. [CrossRef]
37. Wang, D.; Villa, A.; Su, D.; Prati, L.; Schlögl, R. Carbon-supported gold nanocatalysts: Shape effect in the selective glycerol oxidation. *ChemCatChem* **2013**, *5*, 2717–2723. [CrossRef]
38. Sanchez, F.; Alotaibi, M.H.; Motta, D.; Chan-Thaw, C.E.; Rakotomahevitra, A.; Tabanelli, T.; Roldan, A.; Hammond, C.; He, Q.; Davies, T.; et al. Hydrogen production from formic acid decomposition in the liquid phase using Pd nanoparticles supported on CNFs with different surface properties. *Sustain. Energy Fuels* **2018**, *2*, 2705–2716. [CrossRef]

39. Franklin, R.E. Homogeneous and heterogeneous graphitization of carbon. *Nature* **1956**, *177*, 239. [CrossRef]
40. Chen, X.; Deng, X.; Kim, N.Y.; Wang, Y.; Huang, Y.; Peng, L.; Huang, M.; Zhang, X.; Chen, X.; Luo, D.; et al. Graphitization of graphene oxide films under pressure. *Carbon N. Y.* **2018**, *132*, 294–303. [CrossRef]
41. Wilgosz, K.; Chen, X.; Kierzek, K.; Machnikowski, J.; Kalenczuk, R.J.; Mijowska, E. Template method synthesis of mesoporous carbon spheres and its applications as supercapacitors. *Nanoscale Res. Lett.* **2012**, *7*, 269. [CrossRef]
42. Andreas, H.A.; Conway, B.E. Examination of the double-layer capacitance of an high specific-area C-cloth electrode as titrated from acidic to alkaline pHs. *Electrochim. Acta* **2006**, *51*, 6510–6520. [CrossRef]
43. Tasis, D.; Tagmatarchis, N.; Bianco, A.; Prato, M. Chemistry of Carbon Nanotubes Chemistry of Carbon Nanotubes. *Chem. Rev.* **2006**, *106*, 1105–1136. [CrossRef]
44. Bonanni, A.; Pumera, M.; Miyahara, Y. Influence of gold nanoparticle size (2-50 nm) upon its electrochemical behavior: An electrochemical impedance spectroscopic and voltammetric study. *Phys. Chem. Chem. Phys.* **2011**, *13*, 4980–4986. [CrossRef] [PubMed]
45. Pifferi, V.; Chan-Thaw, C.; Campisi, S.; Testolin, A.; Villa, A.; Falciola, L.; Prati, L.; Pifferi, V.; Chan-Thaw, C.E.; Campisi, S.; et al. Au-Based Catalysts: Electrochemical Characterization for Structural Insights. *Molecules* **2016**, *21*, 261. [CrossRef] [PubMed]
46. Grdeń, M.; Łukaszewski, M.; Jerkiewicz, G.; Czerwiński, A. Electrochemical behaviour of palladium electrode: Oxidation, electrodissolution and ionic adsorption. *Electrochim. Acta* **2008**, *53*, 7583–7598. [CrossRef]
47. Maiyalagan, T.; Scott, K. Performance of carbon nanofiber supported Pd–Ni catalysts for electro-oxidation of ethanol in alkaline medium. *J. Power Sources* **2010**, *195*, 5246–5251. [CrossRef]